CHAPTER V

STRUCTURE AND METAMORPHISM

STRUCTURE

Central Crystallines form a major tectonic unit delineating the Higher Himalaya resting over the Lesser Himalayan rocks, and the tectonic plane separating the two was recognised and designated as the Main Central Thrust (MCT) in Kumaun Himalaya as well as in other parts of the Himalaya (Heim and Gansser, 1939; Gansser, 1964; Bordet, 1973; Virdi, 1981; Thakur, 1981; Bahuguna and Saklani, 1988; Fuchs, 1975). Valdiya (1973) postulated yet another thrust in the Higher Himalaya of Kumaun region at a higher tectonic level than the MCT of Heim and Gansser (1939) and named it as 'Vaikrita Thrust'. This thrust was further identified by him (Valdiya, 1980, 1988, 1991, 1993) as the Main Central (Vaikrita) (MC (V) T) Thrust.

The original MCT earlier delineated by Heim and Gansser (1939) at a lower tectonic level was redesignated as the Munsiari Thrust by Valdiya (1980). Sharma (1977) and Thakur (1980) traced the Vaikrita Thrust in eastern Himachal Pradesh. The MC(V)T is too, controversial and Mehdi et al. (1972) and Virdi (1980) have questioned the existence of this thrust. While the MCT (of most workers) marks the southern limit of the Central Crystallines, the northern limit is bounded by the steep Malari Thrust, regionally described as the Trans Himadri Thrust by Valdiya (1987, 1988b). Between these two tectonic lineaments occur the huge lithotectonic slab thrusted upto great heights.

On a regional scale considerable structural data has been generated on the MCT and the Central Crystallines of Kumaun Himalaya and the broad details of the structural set up of the area are available (Misra and Bhattacharya, 1976; Valdiya, 1973, 1978, 1979, 1980, 1987, 1988, 1991, 1993; Thakur, 1981; Chamyal, 1987; Roy and Valdiya, 1988; Chamyal and Vashi, 1989; Chamyal and Manudip, 1994). In this study, the author has not been able to go into details of the structural history of the Central Crystallines of Kumaun Himalaya, but with a view to provide appropriate background a generalised picture of the structural characteristics of the granitoids and associated rocks has been worked out. A structural trend map of the Pindar Sarju, Ramganga, Gorigamga and Darmaganga valleys (Fig.V.1) and the cross-sections

(Figs.III.2,4,6,8) are prepared to give an bird eye view of the structural setting of the region.

The rocks of the Central Crystallines have undergone polyphase deformation, with imprints of each deformational event preserved in them (Chamyal and Manudip, 1994). The fold history of the crystallines of the Higher Kumaun Himalaya and as well as of the various Lesser Himalayan nappes is summarised in Table V.1. The structural history of the Lesser Himalayan Crystalline nappes is found similar (Chamyal and Vashi, 1989). It is obvious as these have been identified to comprise remnants of synformally folded Central Crystalline thrust sheet (Auden, 1937; Heim and Gansser, 1939; Gansser, 1964).

ISOCLINAL/RECLINED FOLDING

The first two foldings (F_1 and F_2) recorded in the Central Crystallines as well as in the various Crystalline nappes of the Lesser Himalaya are co-axial, having identical geometry with variable plunges towards NNE-NE/SSW-SW and are represented by the tight isoclinal/reclined folds (Plates V.1,2).

The main schistosity of the rocks is generally seen to represent axial plane cleavage of F_2, though relicts of the earlier axial plane foliation related to F_1 are abundantly recorded. Most of the granitoid bands ideally show F_1 and F_2 folds at mesoscopic as

Table V.1 : The fold history of the Central Crystallines in Kumaun.

Event	Nature	Central Crystallines Pindar/Sarju/Ramganga Goriganga/Darmaganga valleys	Crystalline Nappes Almora/Baijnath/ Askot/Dharamgarh Chiplakot	Trend
F_1	Isoclinal/ Reclined	Present	Present	NNE-NE/ SSW-SW
F_2	Isoclinal/ Reclined	Present	Present	NNE-NE/ SSW-SW
F_3	Synformal folding	Present	Present	NW-SE
F_4	Flexural folding	Present	Present	NE-SW

Plate V.1 F_2 fold in augen gneiss at Kalamuni, Goriganga Valley

Plate V.2 Quartzo-feldspathic veins folded on F_2 near Munsiari, Goriganga Valley well as at microscopic scales (Plates V.1 and 2). Hence, it is reasonable to conclude that the granitisation precluded the F_1 and F_2 fold episodes. The granitoids which are involved in F_1 and F_2 constitute F_1 fold cores refolded on F_2. These F_1 and F_2 folds are also preserved in the quartzites and quartz rich variety of schists (Plates V.3). The hinge portions of these mesoscopic folds are generally thick and the limbs are thin. The rootless and tight folds of F_1 and F_2 generation are more intense in the thrust zone. According to Merh (1984) and Chamyal and Vashi (1989) F_1 and F_2 foldings are pre-Himalayan and of Precambrian age. The axial planes of these folds have a regional strike WNW-ESE with moderate northerly dips.

The dominant schistosity (S_2) and the related planar structures characterise the axial plane direction of F_2. That S_2 is derived from S_1, is ideally shown in some thin sections of mica-schists, that reveal tight chevron folds (micro-crinkles) (Plate V.3). The linear structures L_1 and L_2 related to F_1 and F_2; are the axes of the microscopic folds in quartz and quartzofeldspathic veins, which many a time are rolled into rods; axes of the banding of stretched quartz veins; orientation of mica flakes along S_0/S_1 and S_2 intersections; and the axes of the reclined crinkles. The two tectonic units (Munsiari and Vaikrita) of Valdiya (1977) as per Roy and Valdiya (1988) show different structural patterns. The author however could not record any change in the structural trends.

THRUSTING

A thrust movement along the pre-existing lineament (MCT) pushed the crystallines over the Lesser Himalayan rocks (Chamyal and Vashi, 1989; Chamyal and Manudip, 1994). The MCT is essentially a Pre-Himalayan tectonic feature (Sychanthavong and Merh, 1984; Chamyal et al., 1984). According to Merh (1984) this major tectonic lineament developed during the waning phase of Hercynian orogeny on account of crustal stretching and rifting, the mechanism related to a process of obduction along the northern flank of the subducted mid-oceanic ridges. The Central Crystallines, thus comprise a tectonic flake demarcated by MCT, a dislocation developed within the Indian Precambrian shield under collisional compressive slicing mechanism (Oxburg, 1972).

The MCT in Kumaun trends E-W to NW-SE dipping due N to NE. The movement along this thrust has not only sheared the rocks but has also given rise to a new set of folds (related to the drag effect) superimposed over the Precambrian deformation (Plate V.4). As the drag folds also show a NNE to NE axes, it appears that the major movement along MCT was from NW. Besides the drag folds, rootless and tight folds are also observed in the vicinity of the thrust with their plunge in the same direction (NNE to NE or SSW to SW). They have folded the schistosity (S_2) and their axes marks the thrust related linear structure (L_T) while the phyllonitic cleavage represents the planar structure (S_T). The fact that the F_1, F_2 folds

Plate V.3 Photomicrograph showing F_2 folds (Crossed Nicols X 40)

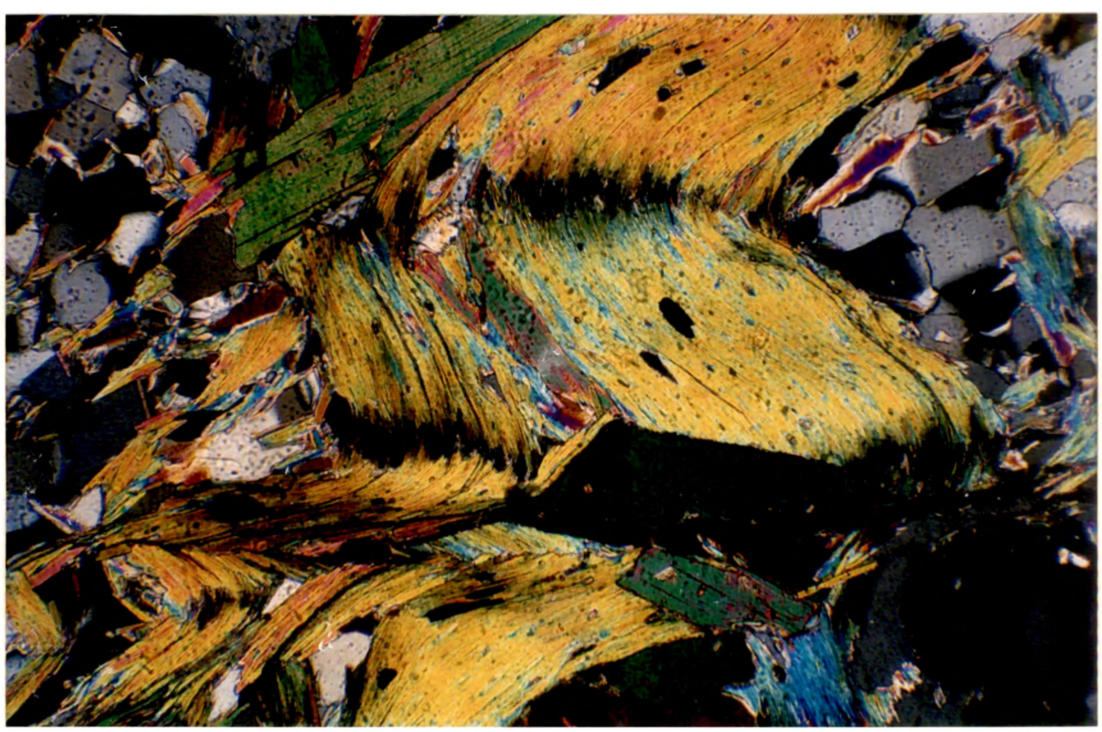

Plate V.4 Photomicrograph showing drag folds (Crossed Nicols X 60) and the thrust related drag folds show similar trends (Chamyal and Manudip, 1994), is not yet fully understood. Perhaps it is just a coincidence.

SYNFORMAL FOLDING

The next fold episode (F_3) is essentially a Tertiary event related to the Himalayan uplift. It is this folding which is held responsible for the folding of the crystalline thrust sheet into various synformal nappes (Vashi and Merh, 1974; Chamyal and Vashi, 1989). The F_3 folds show NW/SE trend and are open in nature, related to this are various mesoscopic synformal nappes with asymmetrical and parasitic folds. F_3 folding has also given rise to extensive crinkling (Plate V.5) of the schists and is almost at right angles to F_1 and F_2. The planar structure related to F_3 includes the axial plane cleavage S_3 trending NW/SE. The most significant phenomenon related to this folding and very well exhibited in the vicinity of the various crystalline thrusts is development of a strong striation lineation ('a'), trending NE and perhaps owes its origin to the effect of flexural slip during F_3 (Chamyal and Vashi, 1989; Chamyal and Manudip, 1994). The lineation at places is marked by slickensides, stripping and stretching of minerals in a direction normal to the F_3 axial trend (Chamyal et al., 1984).

FLEXURAL FOLDING

The F_4 which is the last fold episode has imparted only waviness to the regional foliation trends (Plate V.6). The folds are open to chevron, trending NNE-NE/SSW-SW. The planar elements related to F_4 include the axial plane cleavage S_4 trending NE-SW and also the crenulation axes of F_4 (L_4) trending NE/NNE-SW/SSW with deviation towards N-S direction.

Almost all over the Himalaya are observed transverse faults trending N-S, NNW-SSE, NNE-SSW. They have even dislocated the MCT and perhaps represent the last deformational event in the Himalayas (Valdiya, 1976).

Roy and Valdiya (1988) while describing the tectonometamorphic evolution of the Kumaun Higher Himalaya classified the small scale structures into two types - (i) folds parallel to lineation and (ii) folds at high angles to lineation. According to these workers F_1 and F_2 folds (and their subtypes) formed under different tectonic conditions and the terms F_1 and F_2 do not imply the chronological order of their formation, but are descriptive terms indicating the orientation of the axes and axial planes of the folds in relation to the direction of tectonic transport. However, Chamyal and Vashi (1989) and Chamyal and Manudip (1994) find it difficult to agree with this statement. They have assigned Precambrian ages to F_1 and

Plate V.5 Photomicrograph showing F_3 folds (Crossed Nicols X 40)

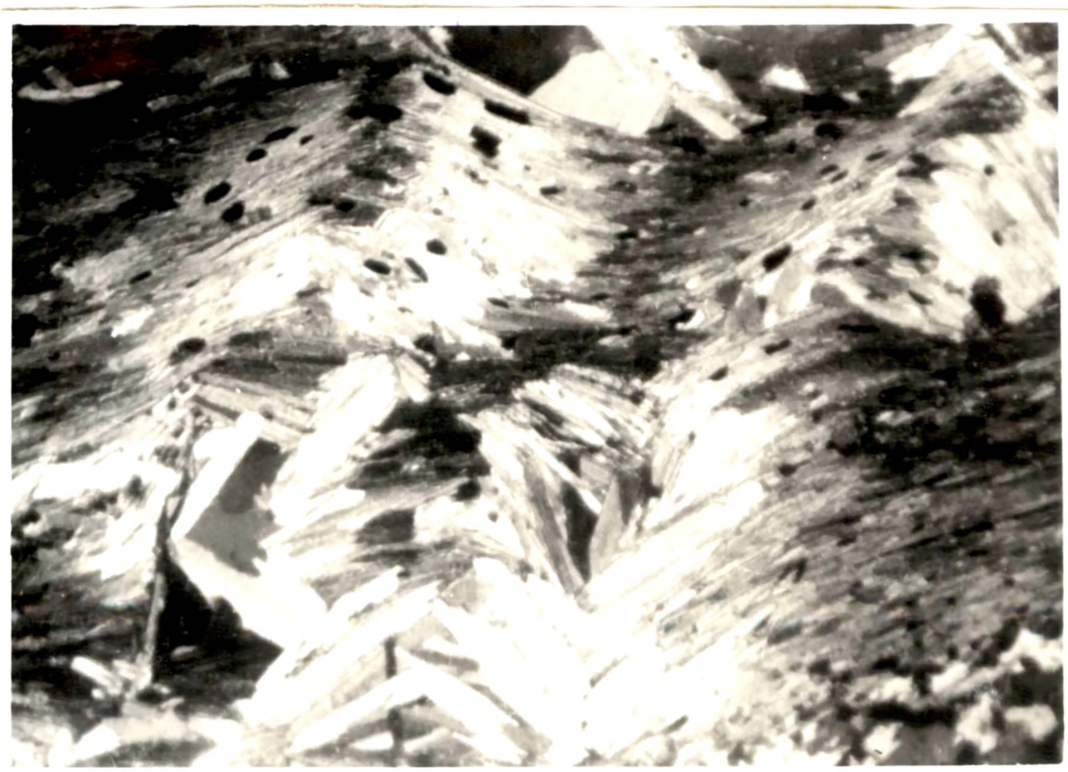

Plate V.6 Photomicrograph showing open folds related to F_4 (Crossed Nicols X 40)

F_2 (which are part and parcel of the Precambrian orogenic event), and Himalayan to Late-Himalayan ages to F_3 and F_4.

METAMORPHISM

From the metamorphic angle too, the Central Crystallines show polyphased metamorphism (Pande and Saxena, 1968; Powar, 1972; Gairola, 1975; Gairola and Ackermand, 1984; Thakur and Chaudhary, 1983; Chamyal, 1984). The textural as well as field studies reveal that these rocks have suffered metamorphism ranging upto upper amphibolite facies. According to Merh (1984) and Chamyal and Vashi (1989) the Crystalline Group of rocks of Kumaun show a metamorphic history, extending from the Precambrian times to as late as the Tertiary.

The rocks of the Higher Kumaun Himalaya (Central Crystallines) exhibit metamorphic characters that indicate mainly two progressive phases followed by retrogression. In the vicinity of the various thrusts (Main Central Thrust, Baijnath Thrust, North and South Almora Thrusts, Dharamgarh Thrust, North and South Chiplakot Thrusts and Askot Thrust) a gradual decrease in metamorphism is observed. The mineralogy, texture and structure of these rocks reveal metamorphic changes that synchronise with the successive deformational events, Pre-Himalayan as well as Himalayan (Chamyal, 1984). The relation between the various deformational episodes with attendant metamorphic events in the Sarju, Pindar, Ramganga, Goriganga and Darmaganga valleys has been worked out by the present author (Table V.2).

METAMORPHIC EVENT (M)

Very limited data is available on this earliest metamorphic event, owing to obliteration of the evidences. However, evidences do point to the existence of a metamorphic event prior to F_1 folding under microscope. Extensive crinkling of mica flakes is conclusive indication of the existence of an early micaceous foliation, which was later on involved in F_1 folding.

METAMORPHIC EVENT (M_1)

The granitisation and formation of the granitoid rocks within the crystallines, perhaps comprised a phenomenon related to this metamorphic event. With increasing depth, the earlier rocks might have changed over to granitoids. The field setting of the granitoid rocks pointing to successive stages of increased granitisation and the existence of more than one granitoid bands within the schists, do point out to the following facts :

1. The involvement of granitoid rocks in F_1 folding,
2. The pre – F_1 granitisation could be part and parcel of the earlier metamorphism M.

Table V.2 Relation between the deformational episodes with attendant metamorphic changes.

Deformation	Metamorphic event	Metamorphism/Metamorphic Products
Load	M	Development of bedding cleavage, minerals unknown.
Isoclinal folding (F_1)	M_1	Development of schistosity S_1 and gneissic foliation, granitisation and formation of granitoids,
Isoclinal folding (F_2)	M_2	Development of main schistosity S_2, growth of snowball garnets, change over of basic rocks to amphibolites, involvement of granitoid rocks in F_2 folding.
Movement along thrust and related drag folding (F_T)	M_T	Development of phyllonites, chlorite, sericite schists, granulation and fracturing of quartz and development of strain shadows in quartz grains.
Synformal folding (F_3)	M_3	Crinkling of the foliation S_2 and development of strain-slip cleavage S_3, formation of new garnet, of muscovite and biotite porphyroblasts along axial planes of the crinkles.
Open flexuring F_4	M_4	Development of minor open folds and formation of biotite and muscovite flakes.

This is recorded by the appearance of abundant plagioclase in the groundmass of the feldspathic schists. In the advanced stages augen and ultimately porphyroblastic gneisses were formed due to increasing activity of potassic emanations over sodic emanations. A number of plagioclase porphyroblasts are gradually replaced by microcline because of increasing potassic content in the porphyroblastic variety. Studies on similar rocks in the various synformal nappes by various workers (Pande, 1963; Powar, 1972; Merh and Vashi, 1965) have furnished interesting details about the processes of granitisation. The undoubted involvement of the gneissic bands in F_1 isoclinal folding in Almora Crystallines (Karanth, 1977, 1985) adequately establishes that the granitisation was pre-F_1 and obviously Precambrian. The available geochronological data on the gneissic rocks also points to their being Precambrian age (Bhanot et al., 1977; Pande et al., 1986).

METAMORPHIC EVENT (M_2)

The most conspicuous and widespread metamorphism that synchronised with the isoclinal folding (F_2), is of regional dynamothermal type. The event is characterised by the development of the axial plane schistosity (S_2), growth of snowball garnets, and kyanites. The mineral assemblages of the various rock types suggests that M_2 was a regional phenomenon, with the maximum grade of metamorphism being of upper amphibolite facies. The most striking textural feature of S_2 recorded is the microfolding of the earlier cleavage S_1. Tightly folded mica flakes define the S_2 plane and in the hinge zones of the F_2 folds most of the micas are re-aligned parallel to the main traces of S_2 foliation. The recrystallization of the quartz and mica reflects the effect of M_2 metamorphism. The garnet porphyroblasts of M_2 generation show a syntectonic rotational growth. The garnets with spirally arranged inclusions indicate the role of differential slipping during its growth, which is synchronous with the F_2 folding.

METAMORPHIC EVENT (M_T)

This event is well evidenced in the vicinity of MCT and other thrusts, bounding various crystalline nappes. It is characterised by the conspicuous phenomenon of retrogression (M_T) along the thrust planes; the rocks along which have been diaphthorised to phyllonites and chlorite schists. Obviously, the retrogression is due to the largescale movement of the Central Crystallines along the MCT. The downgrading of the metamorphism is reflected even in the rocks which are away from the thrust zone and the phenomenon is revealed by the following changes :

1. Granulation and fracturing of quartz,
2. Development of strain shadows in quartz grains,
3. Chloritization of garnet and biotite,
4. Sericitization of muscovite,

5. Formation of fine grained phyllonites from the coarse to medium grained garnet mica schists, along some thrust related shear zones.

The effect of the metamorphic event diminishes progressively on moving away from the thrust northwards.

METAMORPHIC EVENT (M_3)

This metamorphic event, once again has produced progressive metamorphic changes, but on a limited scale, and is related with the F_3 folding. Development of strain-slip cleavage (S_3) is seen sporadically in quite a few sections and is characterised by the growth of new mica and formation of new garnets during F_3. Desai (1968), Patel (1971) and Shah (1972) have also described development of this strain-slip cleavage and growth of new garnets in the Almora Crystallines. It is during this metamorphism that the sericite and chlorite recrystallised into porphyroblastic flakes of muscovite and biotite respectively, which show oblique relationship with the main foliation S_2 and define S_3.

METAMORPHIC EVENT (M_4)

This event has not brought any significant metamorphic changes. As it coincides with the F_4 fold episode which produced open flexures, some of the biotite and muscovite flakes could have formed during this episode.

GEOTHERMOMETRY

The prevailing temperature conditions during metamorphism can be estimated by comparing the natural mineral assemblages with experimentally determined mineral equilibria assuming that the mineral assemblages and reactions were in equilibrium. Thermodynamic properties of partitioning of elements in coexisting minerals can be brought out with the help of electron microprobe (EPMA) data of metamorphic rocks.

The author carried out her studies in the laboratories of N.G.R.I., Hyderabad for obtaining the EPMA data, thin sections (46 mm in length and 25-30 thickness) were prepared and polished on both the sides. Each section was coated with carbon film (100-150 A^0 thick) for uniform electrical conductivity. Mineral analyses was done by using a CAMCEA make, Came box micromode EPMA with an online PDP 11/03 computer. Regress 'ZAF' correction procedure as modified by Henock and Maurice (1978) was used. The absolute error is 2% of the amount present for the major elements. Analyses was done at an accelerating voltage of 15 kv, 6.2 nA sample current and the diameter of the electron beam was approximately 1μ with a counting time of 10 seconds for each element. The standards used were : albite for Na_2O, orthoclase for K_2O, wollastonite for CaO and SiO_2, synthetic MgO for MgO, synthetic Cr_2O_3 for Cr_2O_3, Synthetic Mn TiO_3 for MnO and TiO_2, synthetic hematite for Fe_2O_3.

Many models of geothermometers have been proposed for the estimation of temperatures during metamorphism. Some of these models were applied to four samples of granitoid rocks, three from Central Crystallines and one from the Almora Crystalline nappe, keeping in mind the mineralogical assemblage of these rocks. Data obtained by microprobe analyses for these samples are given in Tables V.3, 4, 5 and 6.

Stormer (1975) formulated a geothermometer based on the partitioning of the albite component between plagioclase and alkali feldspar. He used published Margules parameters to obtain a simple expression relating the composition of co-existing feldspars to temperature :

$$T\ (^{\circ}K) = \frac{\{6326.7 - 9963.2\, X_{AF} + 943.3\, X_{AF}^2 + 2690.2\, X_{AF}^3 + (0.0925 - 0.1458\, X_{AF} + 0.0141\, X_{AF}^2 + 0.0392\, X_{AF}^3)P\}}{(-1.9872 \ln X_{AF}/X_{PL} + 4.6321 - 10.815\, X_{AF} + 7.7345\, X_{AF}^2 - 1.5512\, X_{AF}^3)}$$

Later on Whitney and Stormer (1977) proposed yet another geothermometer based on the partitioning of $NaAlSi_3O_8$ between co-existing microcline and plagioclase solid-solutions. This model

Table V.3 Representative microprobe analyses of minerals of Sample No. M17 from Higher Kumaun Himalaya

	Garnet				Muscovite			Plagioclase			K-Feldspar	
	Core	Rim	Core	Rim	Core	Rim	Core	Core	Rim	Core	Rim	Core
SiO2	34.84	34.37	35.14	35.31	46.82	46.36	46.45	66.77	67.21	67.04	63.88	64.02
TiO2	0.02	0.07	0.18	0.04	0.53	0.53	0.38	–	0.02	0.02	–	0.03
Al2O3	21.55	20.91	20.83	20.87	34.13	34.17	34.21	21.18	20.91	21.35	18.65	18.77
FeO(T)	32.08	34.10	30.96	33.60	3.88	3.73	3.79	0.06	–	0.02	0.03	–
MnO	10.15	9.59	11.95	9.51	0.08	0.15	0.02	0.03	0.02	–	–	–
MgO	0.22	0.27	0.30	0.30	0.48	0.39	0.48	–	–	0.02	–	0.03
CaO	0.96	0.79	–	0.85	–	–	–	1.27	1.03	1.48	–	–
Na2O	0.04	–	0.19	–	0.43	0.37	0.28	9.65	9.64	9.68	0.60	0.79
K2O	0.05	–	0.08	0.09	10.61	10.66	10.35	0.21	0.21	0.19	15.68	15.34
Cr2O3	–	0.03	0.04	0.07	–	0.06	0.04	0.07	0.08	0.06	0.04	0.01
NiO	0.02	–	–	0.03	0.01	–	0.06	0.03	–	–	0.12	0.01
Total	99.93	100.13	99.67	100.67	96.97	96.42	96.06	99.27	99.16	99.86	99.00	99.00
	Cations based on 12 oxygens				Cations based on 20 oxygens			Cations based on 8 oxygens				
Si 4+	2.890	2.870	2.926	2.918	6.206	6.182	6.202	2.935	2.953	2.930	2.982	2.980
Al/Al^{IV}	–	–	–	–	1.794	1.818	1.798	–	–	–	–	–
Al^{VI}	2.107	2.058	2.044	2.032	3.537	3.552	3.585	1.097	1.082	1.100	1.026	1.030
Ti 4+	0.001	0.004	0.011	0.002	0.053	0.053	0.038	0.000	0.001	0.001	0.000	0.001
Fe 2+	2.225	2.381	2.156	2.322	0.430	0.416	0.423	0.002	0.000	0.001	0.001	0.000
Mn	0.713	0.678	0.843	0.666	0.009	0.017	0.002	0.001	0.001	0.000	0.000	0.000
Mg	0.027	0.034	0.037	0.037	0.095	0.078	0.096	0.000	0.000	0.001	0.000	0.002
Cr	0.000	0.002	0.003	0.005	0.000	0.006	0.004	0.002	0.003	0.002	0.001	0.000
Ca	0.085	0.071	0.000	0.075	0.000	0.000	0.000	0.060	0.048	0.069	0.000	0.000
Na	0.006	0.000	0.031	0.000	0.110	0.096	0.072	0.822	0.821	0.820	0.054	0.071
K	0.005	0.000	0.008	0.009	1.794	1.813	1.763	0.012	0.012	0.011	0.934	0.911
Total	8.059	8.098	8.059	8.066	14.028	14.031	13.984	4.931	4.921	4.934	4.998	5.634

Table V.4 Representative microprobe analyses of minerals of Sample No. A2 from Lesser Kumaun Himalaya (Almora Crystallines)

	Muscovite				Biotite						Plagioclase				K-Feldspar				
	Core	Rim	Rim	Core	Core	Rim	Core	Rim	Core	Rim	Core	Rim	Core	Rim	Core	Core	Core	Core	Rim
SiO2	46.66	46.97	45.70	45.78	34.38	34.84	34.41	34.52	34.64	34.89	65.54	64.82	63.77	64.22	64.95	67.13	64.57	64.29	65.27
TiO2	0.86	1.02	0.62	0.00	2.91	3.04	2.94	2.99	3.20	3.05	-	-	-	0.02	0.02	0.04	-	0.07	0.02
Al2O3	35.87	35.74	36.22	37.48	19.72	18.96	18.64	18.68	19.25	18.93	21.52	23.12	23.42	22.68	19.14	20.16	18.53	19.40	18.64
FeO(T)	1.72	2.17	1.89	1.85	25.55	25.30	24.47	24.41	25.33	24.97	0.12	0.01	0.06	0.14	0.03	0.07	0.04	0.04	-
MnO	-	0.06	0.08	0.03	0.33	0.34	0.35	0.39	0.27	0.30	0.01	0.01	0.01	-	0.02	0.04	0.01	0.01	-
MgO	0.60	0.82	0.74	-	5.28	5.01	5.10	5.20	5.35	5.33	-	0.01	-	0.01	0.04	-	0.05	0.03	0.02
CaO	0.01	0.03	0.04	-	0.01	0.02	-	0.01	-	-	1.45	3.09	3.88	3.34	-	1.04	-	-	-
Na2O	0.42	0.40	0.56	0.32	0.17	0.15	0.10	0.06	0.12	0.16	9.45	8.41	8.17	8.36	1.21	9.45	1.07	1.14	1.11
K2O	10.06	9.88	10.21	9.93	9.54	9.12	9.14	8.99	8.86	9.05	0.22	0.27	0.28	0.26	14.15	0.91	14.22	14.22	14.25
Cr2O3	-	0.04	-	0.02	-	0.01	0.06	0.02	0.04	0.02	0.08	-	0.01		0.03	-	0.06	-	0.05
NiO	-	-	0.03	0.04	0.03	0.11	-	-	-	0.01	-	-	-	-	-	0.04	0.02	-	0.03
Total	96.20	97.13	96.09	95.45	97.92	96.90	95.21	95.27	97.06	96.71	98.39	99.74	99.60	99.03	99.59	98.88	98.57	99.20	99.39
	Cations based on 22 oxygen										Cations based on 8 oxygen								
Si 4+	6.140	6.132	6.049	6.056	5.261	5.372	5.368	5.391	5.317	5.373	2.910	2.846	2.814	2.846	2.984	2.969	3.000	2.969	3.005
Al/Al^{IV}	1.860	1.868	1.951	1.935	2.739	2.628	2.614	2.609	2.683	2.627	-	-	-	-	-	-	-	-	-
^{VI}	3.703	3.631	3.699	3.917	0.817	0.818	0.825	0.829	0.800	0.809	1.126	1.197	1.218	1.184	1.037	1.051	1.015	1.056	1.011
Ti 4+	0.085	0.100	0.062	0.000	0.335	0.352	0.346	0.351	0.369	0.353	0.000	0.000	0.000	0.001	0.001	0.001	0.000	0.020	0.001
Fe 2+	0.189	0.237	0.209	0.205	3.269	3.262	3.203	3.187	3.251	3.215	0.004	0.000	0.002	0.005	0.001	0.003	0.002	0.020	0.000
Mn	0.000	0.007	0.009	0.030	0.043	0.044	0.046	0.052	0.035	0.039	0.000	0.000	0.000	0.000	0.001	0.001	0.000	0.000	0.000
Mg	0.118	0.160	0.146	0.000	1.205	1.152	1.190	1.211	1.224	1.224	0.000	0.001	0.000	0.001	0.003	0.000	0.003	0.020	0.001
Cr	0.000	0.004	0.000	0.002	0.000	0.001	0.007	0.002	0.005	0.002	0.003	0.000	0.000	0.000	0.001	0.000	0.002	0.000	0.002
Ca	0.001	0.004	0.006	0.000	0.002	0.003	0.000	0.002	0.000	0.000	0.069	0.145	0.183	0.159	0.000	0.049	0.000	0.000	0.000
Na	0.107	0.101	0.144	0.082	0.050	0.045	0.030	0.018	0.036	0.048	0.813	0.716	0.699	0.718	0.108	0.810	0.096	0.102	0.099
K	1.689	1.645	1.724	1.678	1.862	1.794	1.825	1.791	1.735	1.778	0.012	0.015	0.016	0.015	0.829	0.051	0.843	0.838	0.837
Total	13.892	13.889	13.998	13.888	15.583	15.472	15.472	15.443	15.456	15.468	4.937	4.920	4.932	4.929	4.965	4.935	4.961	4.971	4.956

Table V.5 Representative microprobe analyses of minerals of Sample No. M2b from Higher Kumaun Himalaya

	Muscovite					Biotite							Plagioclase		K-Feldspar	
	Core	Rim	Core	Rim	Core	Core	Rim	Core	Rim	Core	Core	Rim	Rim	Core	Core	Core
SiO2	47.05	47.21	47.68	47.14	47.12	34.71	34.66	34.03	34.57	34.37	34.15	34.75	62.38	62.40	63.59	63.52
TiO2	0.80	0.69	0.61	0.62	0.61	2.47	2.42	2.64	2.65	2.60	2.56	2.39	0.04	0.01	–	0.02
Al2O3	31.24	31.25	31.10	31.58	31.41	17.30	17.48	18.20	17.73	17.40	17.92	17.70	24.25	23.99	18.94	19.45
FeO(T)	3.81	3.83	4.22	4.13	4.07	27.21	27.81	28.51	28.03	28.09	28.12	27.73	0.02	0.10	–	–
MnO	0.08	0.04	0.05	0.12	0.12	0.22	0.22	0.25	0.14	0.25	0.21	0.23	0.05	0.01	0.05	0.03
MgO	1.50	1.34	1.37	1.31	1.47	4.54	4.45	4.29	4.56	4.43	4.56	4.52	–	–	0.06	–
CaO	–	–	–	–	–	–	–	0.02	0.02	–	–	–	4.15	4.29	–	–
Na2O	0.27	0.31	0.61	0.29	0.38	0.19	0.08	–	0.22	0.29	0.18	–	9.07	8.49	0.80	1.03
K2O	10.50	10.53	10.42	10.62	10.72	8.99	9.01	8.89	9.14	9.04	9.38	9.36	0.30	0.22	16.00	15.72
Cr2O3	0.08	0.13	0.04	0.10	0.01	–	–	0.04	0.09	–	–	0.08	0.29	0.22	0.11	0.18
NiO	–	–	0.06	–	0.09	0.04	0.02	–	0.02	–	–	0.04	0.04	–	–	0.11
Total	95.33	95.33	95.71	95.91	96.00	95.67	96.15	96.87	97.17	96.47	97.08	96.80	100.59	99.64	100.55	100.06
	Cations based on 22 oxygen											Cations based on 8 oxygen				
Si 4+	6.348	6.368	6.407	6.335	6.337	5.480	5.456	5.333	5.394	5.410	5.348	5.439	2.749	2.766	2.929	2.942
Al/Al^{IV}	1.652	1.632	1.593	1.665	1.663	2.520	2.544	2.667	2.606	2.590	2.652	2.561	–	–	–	
Al^{VI}	3.315	3.336	3.333	3.336	3.315	0.699	0.699	0.694	0.655	0.638	0.656	0.703	1.260	1.253	1.083	1.062
Ti 4+	0.081	0.070	0.062	0.063	0.062	0.295	0.286	0.311	0.311	0.308	0.301	0.281	0.001	0.000	0.000	0.001
Fe 2+	0.430	0.432	0.474	0.464	0.458	3.592	3.661	3.736	3.657	3.697	3.683	3.629	0.001	0.004	0.000	0.000
Mn	0.009	0.005	0.006	0.014	0.014	0.029	0.029	0.033	0.019	0.003	0.028	0.030	0.002	0.000	0.002	0.001
Mg	0.302	0.269	0.274	0.262	0.295	1.069	1.044	1.002	1.061	1.040	1.065	1.055	0.000	0.000	0.004	0.000
Cr	0.009	0.014	0.004	0.011	0.001	0.000	0.000	0.005	0.001	0.000	0.000	0.010	0.010	0.008	0.004	0.007
Ca	0.000	0.000	0.000	0.000	0.000	0.000	0.000	0.003	0.003	0.000	0.000	0.000	0.196	0.204	0.000	0.000
Na	0.071	0.081	0.042	0.076	0.099	0.058	0.024	0.000	0.067	0.089	0.055	0.000	0.775	0.722	0.071	0.092
K	1.807	1.812	1.786	1.820	1.859	1.811	1.809	1.777	1.819	1.815	1.874	1.869	0.017	0.012	0.094	0.929
Total	14.024	14.018	13.981	14.045	14.092	15.552	15.553	15.561	15.602	15.620	15.661	15.578	5.011	4.969	5.033	5.134

Table V.6 Representative microprobe analyses of minerals of Sample No. M1 from Higher Kumaun Himalaya

	Muscovite					Biotite							Plagioclase		K-Feldspar	
	Core	Rim	Core	Rim	Core	Core	Rim	Core	Rim	Core	Core	Rim	Rim	Core	Core	Core
SiO2	47.05	47.21	47.68	47.14	47.12	34.71	34.66	34.03	34.57	34.37	34.15	34.75	62.38	62.40	63.59	63.52
TiO2	0.80	0.69	0.61	0.62	0.61	2.47	2.42	2.64	2.65	2.60	2.56	2.39	0.04	0.01	-	0.02
Al2O3	31.24	31.25	31.10	31.58	31.41	17.30	17.48	18.20	17.73	17.40	17.92	17.70	24.25	23.99	19.94	19.45
FeO(T)	3.81	3.83	4.22	4.13	4.07	27.21	27.81	28.51	28.03	28.09	28.12	27.73	0.02	0.10	-	-
MnO	0.08	0.04	0.05	0.21	0.12	0.22	0.22	0.25	0.14	0.25	0.21	0.23	0.05	0.01	0.05	0.03
MgO	1.50	1.34	1.37	1.31	1.47	4.54	4.45	4.29	4.56	4.43	4.56	4.52	-	-	0.06	-
CaO	-	-	-	-	-	-	-	0.02	0.02	-	-	-	4.15	4.29	-	-
Na2O	0.27	0.31	0.16	0.29	0.38	0.19	0.08	-	0.22	0.29	0.18	-	9.07	8.40	0.80	1.03
K2O	10.50	10.53	10.42	10.62	10.72	8.99	9.01	8.89	9.14	9.04	9.38	9.36	0.30	0.22	16.00	15.72
Cr2O3	0.08	0.13	0.04	0.10	0.01	-	-	0.04	0.09	-	-	0.08	0.29	0.22	0.11	0.18
NiO	-	-	0.06	-	0.09	0.04	0.02	-	0.02	-	-	0.04	0.04	-	-	0.11
Total	95.33	95.33	95.71	95.91	96.00	95.67	96.15	96.87	97.17	96.47	97.08	96.80	100.59	99.64	100.55	100.06
	Cations based on 22 oxygen												Cations based on 8 oxygen			
Si 4+	6.348	6.368	6.407	6.335	6.337	5.480	5.456	5.333	5.394	5.410	5.348	5.439	2.749	2.766	2.929	2.942
Al/Al^{IV}	1.652	1.632	1.593	1.665	1.663	2.520	2.544	2.667	2.606	2.590	2.652	2.561	-	-	-	-
$_{VI}$	3.315	3.336	3.333	3.336	3.315	0.699	0.699	0.694	0.655	0.638	0.656	0.703	1.260	1.253	1.083	1.062
Ti 4+	0.081	0.070	0.062	0.063	0.062	0.293	0.286	0.311	0.311	0.308	0.301	0.281	0.001	0.000	0.000	0.001
Fe 2+	0.430	0.432	0.474	0.464	0.458	3.592	3.661	3.736	3.657	3.697	3.683	3.629	0.001	0.004	0.000	0.000
Mn	0.009	0.005	0.006	0.014	0.014	0.029	0.029	0.033	0.019	0.033	0.028	0.030	0.002	0.000	0.002	0.001
Mg	0.302	0.269	0.274	0.262	0.295	1.069	1.044	1.002	1.061	1.040	1.065	1.055	0.000	0.000	0.004	0.000
Cr	0.009	0.014	0.004	0.011	0.001	0.000	0.000	0.005	0.011	0.000	0.000	0.010	0.010	0.008	0.004	0.007
Ca	0.000	0.000	0.000	0.000	0.000	0.000	0.000	0.003	0.003	0.000	0.000	0.000	0.196	0.204	0.000	0.000
Na	0.071	0.081	0.042	0.076	0.099	0.058	0.024	0.000	0.067	0.089	0.055	0.000	0.775	0.722	0.071	0.092
K	1.807	1.812	1.786	1.820	1.839	1.811	1.809	1.777	1.819	1.815	1.874	1.869	0.017	0.012	0.940	0.929
Total	14.024	14.018	13.981	14.045	14.082	15.552	15.553	15.561	15.602	15.620	15.661	15.578	5.011	4.969	5.033	5.134

was developed using published Margules parameters for microcline low albite solid solutions. Variations in the structural state of the alkali feldspar as per them could shift the temperature calculated from co-existing feldspar pairs by as much as 100^0 C. The proposed geothermometer can be calculated using the following equation.

$$T(^0K) = \frac{[7973.1-16910.6\ X_{ab,AF} + 9901.9\ X^2_{ab,AF} + (0.11-0.22\ X_{ab,AF} + 0.11\ X^2_{ab,AF})P]}{[-1.9872\ \ln(X_{ab,AF}/a_{ab,PF})+6.48-21.58_{ab,AF} + 23.72\ X^2_{ab,AF} - 8.62\ X^3_{ab,AF}]}$$

Powell and Powell (1977) have argued that the plagioclase alkali feldspar geothermometer formulated by Stormer (1975) does not take into account the effect of small amounts of calcium in the alkali feldspar. This geothermometer was hence reformulated and they showed that as the Ca content of the alkali feldspar increases the temperature calculated using the Stormer geothermometer also increased. Their modified geothermometer is as follows:

$$T = \frac{-x^2_{K,AF}[6330+0.093P+2x_{Na,AF}(1340+0.019P)]}{R\ln K_D+x^2_{K,AF}(-4.63+1.54x_{Na,AF})}$$

While, Haselton et al. (1983) measured heat capacities by adiabatic calorimetry for five highly disordered alkali feldspars. They opined that positive heat capacity deviations from a linear combination of the end member heat capacities, are present mostly at very low temperatures and result in an excess entropy for intermediate compositions. Also that the excess entropy and the volume of mixing was combined with solvus determinations to obtain a calculated enthalpy of mixing, as the measured enthalpies of mixing were essentially coincident with those calculated from the solvus determinations, no short range order for the alkali site could be inferred. Thus they combined the new data for the alkali feldspars with data for plagioclase feldspars to derive an expression for the two-feldspars thermometer that was also consistent with the present knowledge of the thermodynamics of these solid solutions:

$$T_K = \frac{(X^{AF}_{Or})^2(18810 + 17030X^{AF}_{Ab} + 0.364P) - (X^{Pl}_{An})^2 (28230 - 39520\, X^{Pl}_{Ab})}{10.3(X^{AF}_{Or})^2 + 8.3143\ln \{(X^{Pl}_{Ab})^2(2-X^{Pl}_{Ab})/X^{AF}_{Ab}\}}$$

Price (1985) applied the ideal contribution to activity end member or the configurational activity of an end member, to the feldspars to yield an adjustment of the two-feldspar geothermometer. For natural feldspars containing Na, K, Rb, Ca, Ba, Sr and Fe the expression is as follows:

$$T_K = \frac{(X^{AF}_{Or})^2(18810 + 17030\, X^{AF}_{Ab} + 0.364P) - (X^{Pl}_{An})^2 (28230 - 39520\, X^{Pl}_{An})}{10.3(X^{AF}_{Or})^2 + 8.3143\ln \{X^{0,Pl}_{Na}X^{T1,Pl}_{Al}X^{T1,Pl}_{Si}(X^{T2,Pl}_{Si})^2 / X^{0,AF}_{Na}X^{T1,AF}_{Al}X^{T1,AF}_{Si}(X^{T2,AF}_{Si})^2\}}$$

The present author has applied all the above mentioned various two-feldspar geothermometers to the microprobe data for the granitoid rocks of the study area. The results were obtained in the form of temperatures in degree centigrade (Table V.7). Though the results are consistent for these rocks, yet it is obvious that the obtained temperature values are low. This could be attributed to the discrepancy caused by the state of order in high grade metamorphic terranes of the minerals used for calculating the temperatures. At upper amphibolite facies the stable feldspar would probably be orthoclase. But, since order-disorder relations are very sluggish, some order may be inherited from lower temperature state, as in alkali exchange experiments (Whitney and Stormer, 1977).

Using the Ti content in muscovite and biotite calculated from the formula based on 22(o), Lal (1991) formulated a geothermometer which is as follows:

For biotite,

$$T\,^{0}C = [5177/(4.546 - \ln Ti)] - 273.15$$

For muscovite,

$$T\,^{0}C = [9098/(7.789 - \ln Ti)] - 273.15$$

The temperatures obtained by using this geothermometer are furnished in Table V.8, and are found to be consistent with those prevailing in the upper amphibolite facies.

Table V.7 : Temperature estimates for the granitoid rocks

Sample No.	Stormer 1975	Whitney and Stormer 1977	Powell and Powell 1977	Haselton et al. 1983	Price 1985
M 17 at 4 kb	339	473	376	327	326
5 kb	339	473	385	337	336
A 2 at 4 kb	410	543	451	425	424
5 kb	410	543	461	437	435
M 2b at 4 kb	391	528	430	403	402
5 kb	391	528	440	414	413
M 1 at 4 kb	409	550	449	431	428
5 kb	409	550	459	443	439

Table V.8 : Temperature estimates for the granitoids based on Ti content in micas (Lal, 1991).

Sample No.	Biotite	Muscovite
M 17	–	567
A 2	652	611
M 2b	627	596
M 1	621	606